


Article

A Monodisperse Population Balance Model for Nanoparticle Agglomeration in the Transition Regime

Georgios A. Kelesidis¹ and M. Reza Kholghy^{2,*} 

¹ Department of Mechanical and Process Engineering, Eidgenössische Technische Hochschule Zürich, Sonneggstrasse 3, 8092 Zürich, Switzerland; gkelesidis@ptl.mavt.ethz.ch

² Department of Mechanical and Aerospace Engineering, Carleton University, 1125 Colonel by Drive, Ottawa, ON K1S 5B6, Canada

* Correspondence: reza.kholghy@carleton.ca

Abstract: Nanoparticle agglomeration in the transition regime (e.g. at high pressures or low temperatures) is commonly simulated by population balance models for volume-equivalent spheres or agglomerates with a constant fractal-like structure. However, neglecting the fractal-like morphology of agglomerates or their evolving structure during coagulation results in an underestimation or overestimation of the mean mobility diameter, d_m , by up to 93 or 49%, respectively. Here, a monodisperse population balance model (MPBM) is interfaced with robust relations derived by mesoscale discrete element modeling (DEM) that account for the realistic agglomerate structure and size distribution during coagulation in the transition regime. For example, the DEM-derived collision frequency, β , for polydisperse agglomerates is $82 \pm 35\%$ larger than that of monodisperse ones and in excellent agreement with measurements of flame-made TiO₂ nanoparticles. Therefore, the number density, N_{Ag} , mean, d_m , and volume-equivalent diameter, d_v , estimated here by coupling the MPBM with this β and power laws for the evolving agglomerate morphology are on par with those obtained by DEM during the coagulation of monodisperse and polydisperse primary particles at pressures between 1 and 5 bar. Most importantly, the MPBM-derived N_{Ag} , d_m , and d_v are in excellent agreement with the data for soot coagulation during low temperature sampling. As a result, the computationally affordable MPBM derived here accounting for the realistic nanoparticle agglomerate structure can be readily interfaced with computational fluid dynamics in order to accurately simulate nanoparticle agglomeration at high pressures or low temperatures that are present in engines or during sampling and atmospheric aging.



Citation: Kelesidis, G.A.; Kholghy, M.R. A Monodisperse Population Balance Model for Nanoparticle Agglomeration in the Transition Regime. *Materials* **2021**, *14*, 3882. <https://doi.org/10.3390/ma14143882>

Academic Editor: Silvana De Iuliis

Received: 23 May 2021

Accepted: 5 July 2021

Published: 12 July 2021

Publisher's Note: MDPI stays neutral with regard to jurisdictional claims in published maps and institutional affiliations.



Copyright: © 2021 by the authors. Licensee MDPI, Basel, Switzerland. This article is an open access article distributed under the terms and conditions of the Creative Commons Attribution (CC BY) license (<https://creativecommons.org/licenses/by/4.0/>).

Keywords: agglomeration; transition regime; population balance model; discrete element model; fractal-like structure

1. Introduction

Nanoparticles made by gas-phase manufacturing or emitted by incomplete combustion of fossil fuels are abundant in our everyday lives [1]. Incipient nanoparticles grow by coagulation, sintering and surface growth. Inception [2], surface growth [3] and sintering [4] are active only in a narrow window of time, when the temperature is very high. Thus, coagulation is the dominant process in controlling nanoparticle morphology and number concentration, forming fractal-like agglomerates [5]. Such agglomerates are often present at very high concentrations during the gas-phase synthesis of carbon black, ceramic (TiO₂ and SiO₂) and metallic (Ni, Fe and Cu) powders, as well as soot emissions from engines, fires and volcanic plumes [1]. At high pressures or low temperatures that are present in engines [6] or during sampling [7] and atmospheric aging of aerosols [8], these agglomerates are formed by coagulation in the transition regime.

Agglomeration dynamics could be simulated by population balance models if an accurate collision frequency, β , and realistic particle morphologies are employed [5]. For example, sectional population balance models (SPBMs) are used to simulate agglomeration

in the transition regime, with β obtained from the harmonic mean of those in the free molecular and continuum regimes [9] based on the agglomerate gyration, d_g , mobility, d_m , and primary particle, d_p , diameters. The agglomerate structure, quantified by the relation between d_g and d_m [10], changes depending on the number [11], diameter and polydispersity of their constituent primary particles [12]. Accounting for the evolving agglomerate structure with SPBM is not trivial, as multiple equations per section need to be solved [13,14]. Therefore, models for the combustion synthesis of nanomaterials assume that $d_m = d_g = d_p n_p^{0.56}$, based on a constant fractal dimension, $D_f = 1.8$ [15,16] often with a constant value for d_p [17,18]. Similarly, climate models simulate the coagulation dynamics of aerosols assuming that the spheres have the same volume-equivalent diameter, d_v , with nanoparticle agglomerates [19].

With mesoscale discrete element modeling (DEM), the evolution of particle size distribution [3], morphology [10] and collision frequency [20] can be obtained from first principles. For example, it was recently shown that DEM-derived agglomerates reach a quasi-self-preserving size distribution (SPSD) with a mobility-based geometric standard deviation, $\sigma_{g,m} = 1.48 \pm 0.03$ [21], that is narrower than the SPSPD attained in the free molecular regime [12] and in excellent agreement with data for SiO_2 [22] and soot [23,24] agglomerates. The DEM-derived collision frequency of polydisperse agglomerates at their quasi-SPSPD was on average 82% higher than that of monodisperse ones, regardless of the chemical bonding and polydispersity of their constituent primary particles [21]. This DEM-derived collision frequency enhancement is on par with those measured from flame-made TiO_2 nanoparticle agglomerates in the transition regime [21]. Furthermore, power laws relating the mobility diameter normalized by the primary particle diameter, d_m/d_p , or gyration diameter, d_m/d_g , with the number of primary particles per agglomerate, n_p , are derived by DEM simulations in the free molecular and transition regimes [3]. Such power laws can be used in population balance models to estimate accurately the evolving structure of nanoparticles during agglomeration in the transition regime.

Sectional models have been interfaced with computational fluid dynamics (CFD) in order to explain soot formation in diffusion flames [13,14] or predict agglomeration of soot nanoparticles from diesel engine exhausts [7,25]. Finite element methods have also been coupled with SPBMs to simulate coagulation of spheres [26], fractal-like agglomerates [27] and linear stacks (rouleaux) [28]. However, both SPBM and mesoscale simulations are computationally expensive and interfacing them with CFD is not trivial. Monodisperse population balance models (MPBMs) are computationally affordable and easy to use [16,29]. However, they apply best when particles have attained their SPSPD and asymptotic fractal-like structure by coagulation [30]. This is typically the case when high concentrations of nanoparticles coagulate and rapidly attain their quasi-SPSPD [21]. Kruis et al. [16] used a three equation MPBM assuming monodisperse agglomerate and primary particle size distributions to track their coagulation and sintering and compared it to a two dimensional SPBM [31]. The influence of the fractal-like agglomerate structure on its β was accounted for by estimating the agglomerate collision diameter, d_c , using D_f , d_p and n_p . The MPBM predictions agreed well with those of the SPBM for the equivalent primary particle diameter. However, the agglomerate concentration was overpredicted, because the enhancement of β due to the polydispersity of the agglomerate size distribution was not considered. Goudeli et al. [11] interfaced a MPBM with an evolving DEM-derived D_f to elucidate the agglomerate dynamics during coagulation and sintering in the free molecular regime. Neglecting the evolution of D_f hardly affected d_p , but overpredicted the agglomerate collision diameter up to 30% during the transition from hard- to soft-agglomeration (e.g., when the characteristic collision and coalescence times were comparable) [11]. In this regard, the MPBM for coagulation and surface growth [32] was coupled with DEM-derived power laws and coagulation rates in order to accurately describe the dynamics of soot nanoparticles in the free molecular regime. Extending this MPBM for coagulation in the transition regime is essential for the design of cleaner combustion engines, robust sampling

devices for flame-made nanomaterials and accurate climate models for the estimation of the aerosol environmental impact.

The objective of this work is to develop an accurate but computationally affordable MPBM for nanoparticle agglomeration in the transition regime accounting for the evolving agglomerate structure and size distribution. Thus, the DEM-derived quasi-self-preserving size distributions of agglomerates [21] and data-proven power laws governing their structure during their formation in the transition regime [10] are interfaced with a simple and accurate MPBM of their coagulation dynamics. In particular, the coagulation of nanoparticles is elucidated by a MPBM at low and high temperatures and pressures that are relevant during particle formation in engines [6] or sampling [7] and atmospheric aging of aerosols [8]. The collision frequency, number concentration, mobility and volume-equivalent diameters are validated with DEM simulations and data of soot nanoparticles at identical conditions.

2. Theory

2.1. Discrete Element Modeling and Agglomerate Structure

Ballistic and Brownian coagulation dynamics of nanoparticles in the absence of rotation, convection, deposition, van der Waals, electric or hydrodynamic forces are simulated by DEM of agglomeration in the free molecular and transition regimes [20]. This is a serial, event-driven algorithm implemented in C++, as detailed in [20]. In brief, spheres with mean diameter, d_p , of 20 nm and volume fraction of 1 ppm are randomly distributed in a cubic cell at 1 bar and 1830 K. The bulk primary particle density is set to 1800 kg/m³, which is commonly used to simulate the dynamics of mature soot [3] and is close to that of SiO₂ [11]. Particles are in equilibrium with the surrounding gas and change direction after each collision or after traveling their persistence length [33]. The time between collisions is calculated with an event-driven method [34]. Particles stick to each other after collisions and the trajectory of the newly formed agglomerate is calculated by the momentum conservation principle. The surrounding gas pressure, P , is increased from 1 to 5 bar to simulate conditions close to those in combustion engines [6]. The geometric standard deviation, $\sigma_{g,p}$, of the initial particle size distribution is also varied from 1 to 1.5 in order to be consistent with the measured soot [35] and metal oxide [22] primary particle size distributions.

The mobility diameter, d_m , of DEM-derived agglomerates in the free molecular and transition regimes is related to their number of primary particles per agglomerate, n_p , and d_p by [10]:

$$\frac{d_m}{d_p} = n_p^{0.45} \quad (1)$$

and to their diameter of gyration, d_g , by [10]:

$$\frac{d_m}{d_g} = \begin{cases} n_p^{-0.2} + 0.4 & , n_p > 1.8 \\ \sqrt{5/3} & , n_p \leq 1.8 \end{cases} \quad (2)$$

These power laws are obtained for soot particles formed in flames with maximum soot volume fractions spanning two orders of magnitude [10]. Furthermore, Equation (1) has been validated with data of soot, SiO₂, ZrO₂, Au and Ag aerosols [36].

The evolution of the detailed DEM-derived d_m distribution from the free molecular to the transition regime has been validated with data of organic and inorganic nanoparticles from premixed [3], diffusion [21] and spray flames [21]. Figure 1 shows the DEM-derived geometric standard deviation, $\sigma_{g,m}$, of the d_m distribution as a function of the normalized mean, d_m/d_p , of agglomerates, with primary particles having $\sigma_{g,p} = 1$ (a, b: broken lines), 1.2 (a: dotted line) and 1.5 (a: solid line) coagulating at 1830 K, and $P = 1$ (a, b: broken lines), 3 (b: dotted line) and 5 bar (b: solid line). Small $\sigma_{g,p} = 1$ and 1.2 are representative for organic nanoparticles (e.g., soot [3,35]), while $\sigma_{g,p} = 1.5$ is common for inorganic nanoparticles (e.g., SiO₂ [22] and ZrO₂ [37]) that attain their self-preserving size distribution by coalescence. Regardless of $\sigma_{g,p}$, the $\sigma_{g,m}$ of the agglomerate size distribution increases up

to 1.7 ± 0.05 in the free molecular regime at $d_m/d_p = 3$, consistent with DEM simulations of agglomeration and surface growth [10]. At $d_m/d_p > 3$, agglomerates coagulate in the transition regime and their $\sigma_{g,m}$ decreases, asymptotically attaining its quasi-self-preserving $\sigma_{g,m} = 1.48 \pm 0.03$ [21] (thin solid line and shaded area). Increasing P from 1 to 5 bar accelerates the attainment of the $\sigma_{g,m} = 1.48 \pm 0.03$, as agglomerates coagulate mostly in the transition regime at these conditions. The large $\sigma_{g,m}$ attained by coagulation in the free molecular and transition regimes enhances the agglomerate coagulation frequency, as elaborated in the next section.

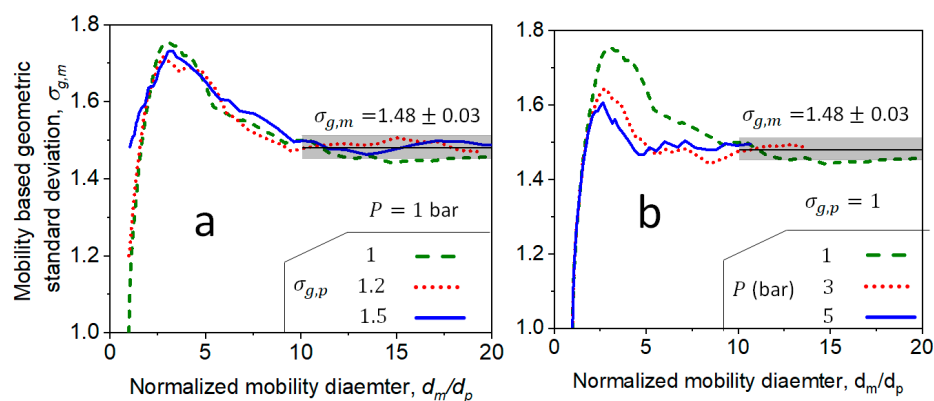


Figure 1. Evolution of geometric standard deviation of agglomerate mobility diameter, $\sigma_{g,m}$, as a function of the normalized mobility diameter, d_m/d_p , during coagulation (a) at $P = 1$ bar for agglomerates consisting of polydisperse primary particles with $1 \leq \sigma_{g,p} \leq 1.5$, and (b) for agglomerates of monodisperse primary particles coagulating at different pressures, $1 \leq P \leq 5$ bar.

2.2. Agglomerate Dynamics With a Monodisperse Population Balance Model

Here, a monodisperse population balance model [16] is implemented in MATLAB (R2020a, MathWorks, Inc., Natick, MA, USA) and used to describe the coagulation dynamics of agglomerates in the transition regime. As the total mass and surface area of the agglomerates are conserved, one equation is enough to track the agglomerate number density and structure. At isothermal conditions, the rate of change in the total agglomerate number concentration, N_{Ag} , is [5]:

$$\frac{dN_{Ag}}{dt} = -\frac{1}{2}\beta_m N_{Ag}^2 \quad (3)$$

where β_m is the collision frequency of monodisperse agglomerates given by the harmonic mean [9]:

$$\beta_m = \frac{\beta_{fm} \cdot \beta_{co}}{\beta_{fm} + \beta_{co}} \quad (4)$$

where β_{fm} is the collision frequency in the free molecular regime [9]:

$$\beta_{fm} = 4\sqrt{\frac{\pi k_B T}{m_{Ag}}} d_c^2 \quad (5)$$

where β_{co} is the collision frequency in the continuum regime [9]:

$$\beta_{co} = \frac{8k_B T}{3\mu} \left(1 + \frac{2\lambda_g}{d_m} (1.257 + 0.4 \cdot \exp(-0.78 \cdot d_m/\lambda_g)) \right) \quad (6)$$

where k_B is the Boltzmann constant, T is the temperature, d_c is the agglomerate collision diameter that is equal to d_p for spheres and d_g for agglomerates (Equations (1) and (2)) to account for their fractal-like structure on β [38], m_{Ag} is the agglomerate mass:

$$m_{Ag} = \rho n_p \pi \frac{d_p^3}{6} \quad (7)$$

where n_p is given by:

$$n_p = \frac{N_{Ag,0}}{N_{Ag}} \quad (8)$$

where $N_{Ag,0}$ is the initial number density of the spherical primary particles. The collision frequency of polydisperse agglomerates, β_p , is related to β_m by [21]:

$$\beta_p = (1.82 \pm 0.35) \cdot \beta_m \quad (9)$$

The average enhancement factor of β_p and its standard deviation have been derived based on 10 DEM simulations of soot and SiO₂ nanoparticle agglomeration at temperatures ranging from 1400 to 1830 K and pressures ranging from 1 to 10 bar [21]. Figure 2 shows the evolution of β as a function of d_m measured (symbols) or estimated (lines and shade) for monodisperse (β_m , Equation (4); broken line) or polydisperse (β_p , Equation (9); solid line and shade) agglomerates of flame-made uncharged or weakly charged TiO₂ nanoparticles with $d_p = 20$ nm at $T = 295$ K [39]. Agglomerates are initially formed by coagulation in the free molecular regime ($Kn > 2.6$). Therefore, their β rapidly increases with increasing d_m . Agglomerates with d_m larger than 100 nm coagulate in the transition regime ($Kn < 2.6$) and their β decreases towards the asymptotic β_{co} in the continuum regime (Equation (6)). The measured β is underestimated up to a factor of 2 by β_m that neglects the polydispersity of the agglomerate size distribution. The Fuchs interpolation for β_m of monodisperse agglomerates in the transition regime results in a similar underestimation of the measured β [39]. In contrast, β_p derived for polydisperse agglomerates [21] is $82 \pm 35\%$ larger than β_m and in excellent agreement with the data. This validates the use of Equation (9) in the MPBM of nanoparticle coagulation in the transition regime.

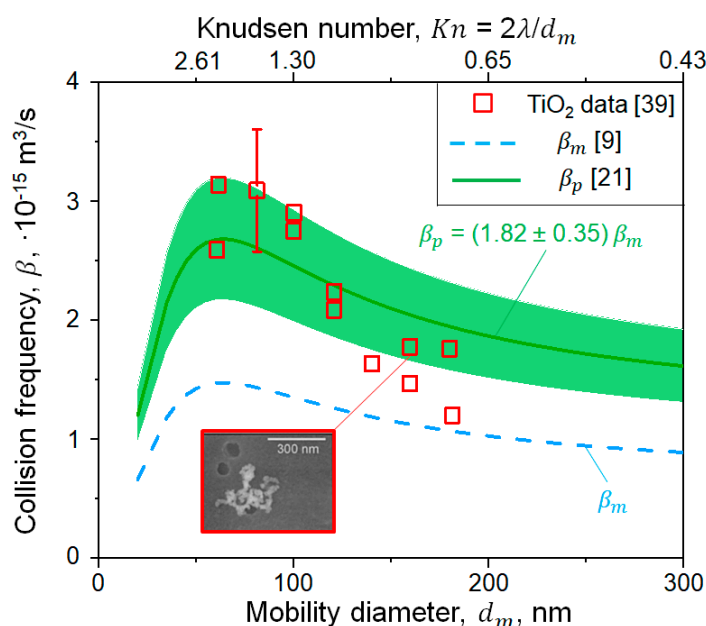


Figure 2. Evolution of collision frequency, β , as a function of agglomerate mobility diameter, d_m (bottom abscissa), or Knudsen number, Kn (top abscissa), measured for flame-made TiO₂ agglomerates (squares, inset) [39] compared to β_m (Equation (4), broken line) and β_p (Equation (9), solid line and shade).

3. Results and Discussion

3.1. Evolution of Agglomerate Morphology by DEM and a MPBM

Figure 3 shows the dynamics of the agglomerate structure quantified by the ratio of the mean mobility diameter over that of gyration, d_m/d_g , as a function of the mean number of primary particles per agglomerate, n_p , obtained by DEM (dotted line and shade) and MPBM (solid line). Particles rapidly evolve from spheres with $d_m = 1.29 d_g$ [40] into agglomerates with $d_m = d_g$ having $n_p \sim 10$, and asymptotically reach $d_m = 0.7 d_g$ [41] as n_p increases. This rapid reduction of d_m/d_g is induced by the enhancement of the agglomerate inertia that determines d_g [42]. Therefore, the agglomerate inertia becomes larger than its drag force at $n_p > 10$ for monodisperse primary particles, resulting in $d_m/d_g < 1$. The DEM-derived evolution of d_m/d_g has been validated with data from wood combustion [10,43]. Most importantly, the agglomerate d_m/d_g estimated here by the MPBM using Equation (2) is in excellent agreement with that obtained by DEM from first principles. This confirms that the MPBM interfaced with DEM-derived power laws accounts for the agglomerate morphology dynamics in detail. Assuming a fixed value for d_m/d_g in the MPBM, such as 1.29 [18], 1 [15] or 0.7 [41], could significantly reduce its accuracy, as $d_m/d_g = 1.29$ is only valid for spheres and $d_m/d_g = 0.7$ is only reached for very large agglomerates [12]. In this regard, using $d_m/d_g = 1$ in the MPBM results in a 49% overestimation of the agglomerate d_m , as discussed in Section 3.4.

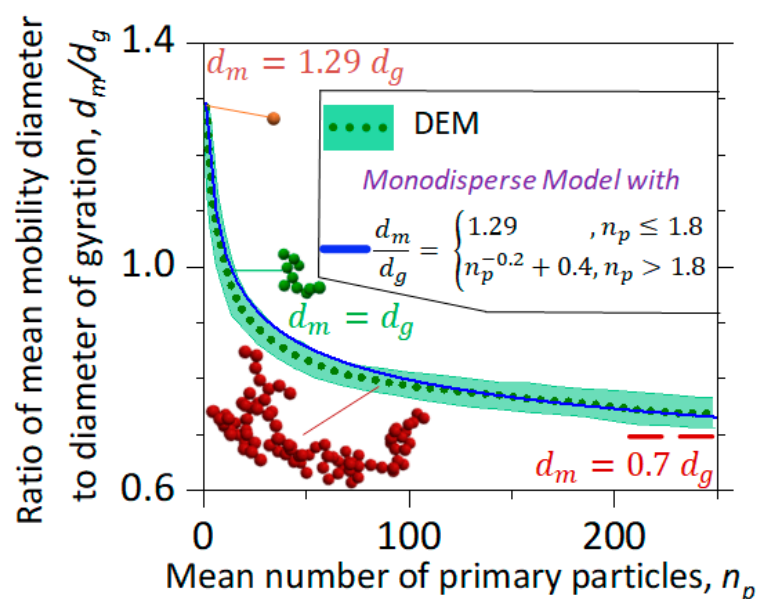


Figure 3. Evolution of the ratio of the mean mobility diameter over that of gyration, d_m/d_g , as a function of n_p during agglomeration derived by DEM (dotted line and green shade) and the MPBM interfaced with Equation (2) (solid line). The d_m/d_g is initially equal to 1.29 for single spheres [40], but rapidly decreases to 1 for agglomerates with $n_p \sim 10$ and $\sigma_{g,p} = 1$ and asymptotically reaches 0.7 (dashed line) for large agglomerates with $n_p \geq 700$ [41]. The DEM-derived relation [10] (solid line, Equation (2)) quantifies the evolution of d_m/d_g within 6% of the DEM simulations.

3.2. Impact of Primary Particle Polydispersity on Agglomeration Dynamics

Figure 4 shows the evolution of (a) collision frequency, β , (b) number density, N_{Ag} , (c) mean mobility, d_m , and (d) volume-equivalent, d_v , diameters as a function of time, t , for agglomerates consisting of primary particles with mean $d_p = 20$ nm and geometric standard deviation, $\sigma_{g,p} = 1$ (broken lines), 1.2 (dotted lines) and 1.5 (solid lines) at $T = 1830$ K and $P = 1$ bar derived by DEM (thick lines) and the MPBM (thin lines and shades). The shades quantify the statistical variation of β_p (Equation (9)).

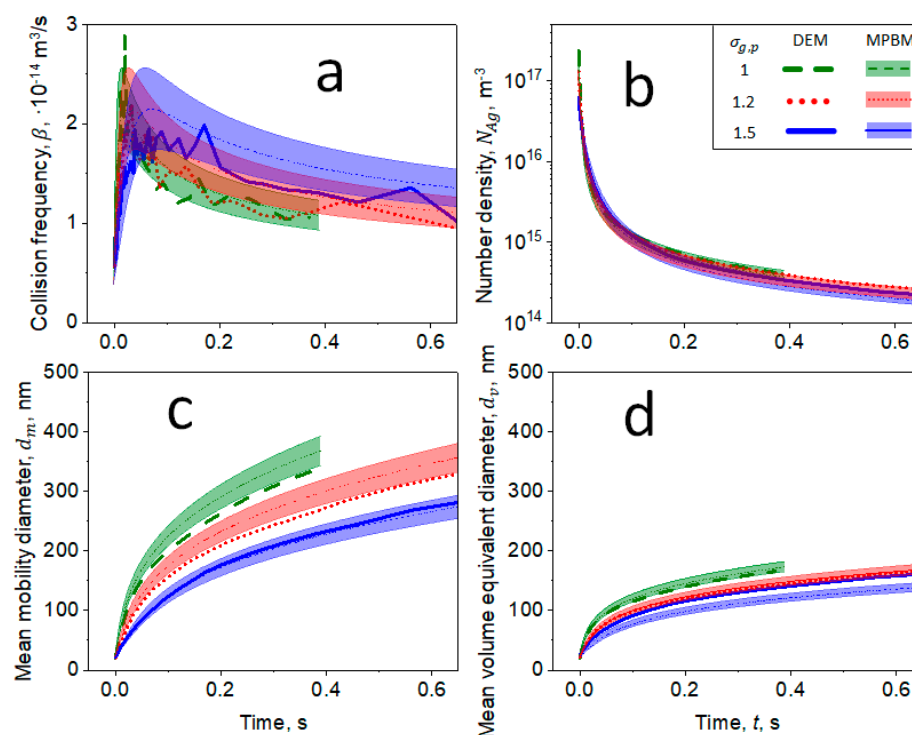


Figure 4. Evolution of (a) β , (b) number density, N_{Ag} , (c) mean d_m and (d) volume-equivalent diameter, d_v , as a function of time, t , for agglomerates consisting of primary particles with mean $d_p = 20$ nm and geometric standard deviation, $\sigma_{g,p} = 1$ (broken lines), 1.2 (dotted lines) and 1.5 (solid lines) at $T = 1830$ K and $P = 1$ bar estimated by DEM (thick lines) and MPBM (thin lines and shades). All sub-figures (a–d) share the same legend.

Increasing $\sigma_{g,p}$ enhances β , resulting in a faster reduction of N_{Ag} with time as shown in Figure 4a. However, increasing $\sigma_{g,p}$ also delays the attainment of the transition regime, as agglomerates consisting of primary particles with larger $\sigma_{g,p}$ have smaller d_m and d_v . This is due to the small primary particles in those agglomerates that have marginal impact on increasing d_m and d_v . The MPBM-derived N_{Ag} , β , d_m and d_v are in excellent agreement with those obtained by DEM for all $\sigma_{g,p}$ investigated here. Therefore, the present MPBM could be used to simulate the coagulation dynamics of organic nanoparticles with rather monodisperse primary particle size distributions [3,35], and also those of metals [44] and metal oxides [22,37] that attain the self-preserving size distribution by coalescence in practical applications. The MPBM-derived agglomeration dynamics are also in excellent agreement with those obtained by DEM for nanoparticles with $d_p = 10, 20$ and 40 nm (Supplementary Materials: Figure S1). The present MPBM has been also validated with DEM simulations and measurements of non-spherical aggregated soot nanoparticles coagulating in the free molecular regime [32].

3.3. Coagulation of Nanoparticles at High Pressures

Figure 5 shows the evolution of (a) β , (b) N_{Ag} , (c) d_m and (d) d_v as a function of t at $P = 1$ (broken lines), 3 (dotted lines) and 5 bars (solid lines) during the coagulation of monodisperse primary particles with $d_p = 20$ nm derived by DEM (thick lines) and the MPBM (thin lines and shades). Agglomerates at 1 bar are initially in the free molecular regime. Thus, their β increases as their n_p and d_g increase rapidly by coagulation. As the agglomerates grow, they enter the transition regime where their β gradually decreases towards an asymptotic value that is rather independent of agglomerate size in the continuum regime [45]. Increasing pressure from 1 to 5 bar decreases β by up to a factor of 2.6, as agglomerate diffusivity decreases at higher pressures [46]. This results in larger N_{Ag} at 3 and 5 bars compared to those obtained at 1 bar. Agglomerate d_m and d_v derived

at 1 bar are at least 50% larger than those obtained at 3 and 5 bar. This is due to their large collision frequency at 1 bar (Figure 5a) that takes place initially in the free molecular regime. Agglomerate d_v is on average 35% smaller than its d_m at all pressures, quantifying the ramified non-spherical agglomerate structure [42]. The MPBM-derived N_{Ag} , β , d_m and d_v are in excellent agreement with those obtained by DEM for all P relevant for soot formation in engines investigated here [6]. The MPBM-derived agglomeration dynamics are also in excellent agreement with those obtained by DEM for initial $N_{Ag,0}$ and (incubation) residence times spanning 6 and 8 orders of magnitude, respectively (Figure S2).

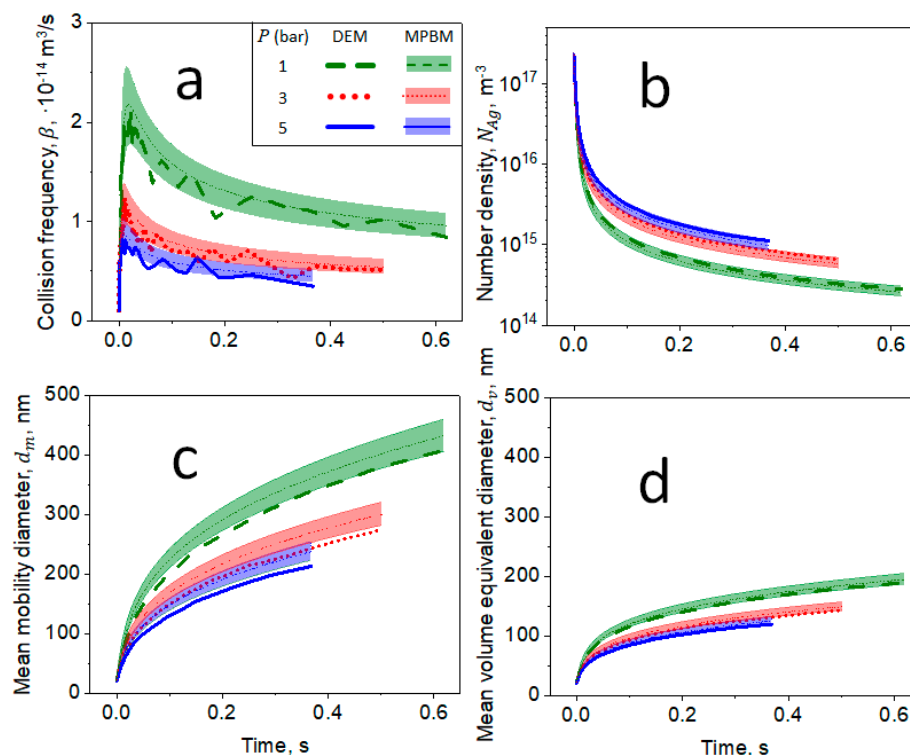


Figure 5. Evolution of (a) β , (b) N_{Ag} , (c) d_m and (d) d_v as a function of t for agglomerates consisting of primary particles with mean $d_p = 20$ nm and $\sigma_{g,p} = 1$ at $T = 1830$ K and $P = 1$ (broken line), 3 (dotted line) and 5 bar (solid line) simulated by DEM (thick lines) and MPBM (thin lines and shades). All sub-figures (a–d) share the same legend.

3.4. Validation of Low-Temperature Coagulation Dynamics with Experiments

Figure 6 illustrates the agglomerate effective density, ρ_{eff} , as a function of the normalized mobility diameter, d_m/d_p , measured for soot particles sampled from premixed ethylene flames with an equivalence ratio (EQR) of 2 (triangles) or 2.4 (squares), and estimated here accounting for the evolving fractal-like agglomerate structure (Equations (1) and (2)) [10], solid line) or assuming a constant agglomerate structure with $d_m = d_g = d_p n_p^{0.56}$ (broken line) [16]. Ramified agglomerates are formed at EQR = 2 and 2.4 having average $d_p = 9$ [35] and 19.6 nm [47], respectively. The agglomerate d_m/d_p increases during coagulation, reducing ρ_{eff} and d_m/d_g from 1.29 to 0.7 (as shown in Figure 3). Neglecting the evolving agglomerate structure and assuming $d_m = d_g = d_p n_p^{0.56}$ underpredicts the measured ρ_{eff} by up to 50%. In contrast, the agglomerate ρ_{eff} obtained here using DEM-derived power laws (Equations (1) and (2)) that account for the realistic agglomerate morphology is in excellent agreement with data of soot nanoparticles from different combustion conditions.

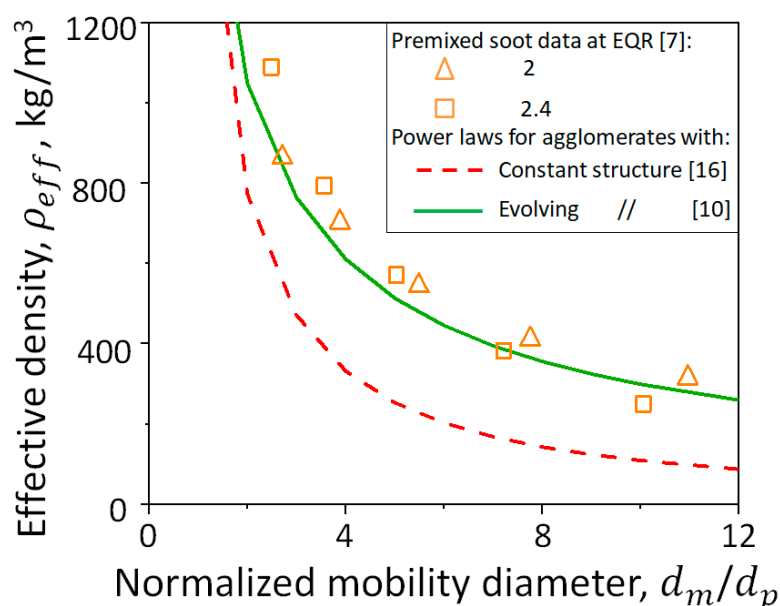


Figure 6. Evolution of agglomerate effective density, ρ_{eff} , as a function of their normalized mobility diameter, d_m/d_p , measured for soot particles sampled from premixed ethylene flames with equivalence ratios of 2 (triangles) or 2.4 (squares) and estimated assuming constant (broken line) or evolving agglomerate structure (solid line).

The impact of the agglomerate morphology on the coagulation dynamics of nanoparticles in the transition regime is investigated next. In particular, Figure 7 shows the agglomerate N_{Ag} (a, b), mean d_m (c, d) and d_v (e, f) of soot nanoparticles measured as a function of t during coagulation at $T = 295$ K (symbols). Soot nanoparticles are sampled from the premixed flames with EQR = 2 (a, c, e) or 2.4 (b, d, f) shown in Figure 7. The measured N_{Ag} , d_m and d_v (symbols [7]) are compared to those estimated by the MPBM (lines, shades) assuming volume-equivalent spheres (dotted lines) or agglomerates with constant (broken lines) or evolving morphology (solid lines).

Approximating agglomerates with volume-equivalent spheres underpredicts their d_m and d_v by up to 93 and 18%, respectively, and overpredicts their N_{Ag} by up to 55%. The N_{Ag} and d_v obtained by the MPBM for agglomerates with a constant or evolving structure are in excellent agreement with the data of soot obtained from both EQRs. However, neglecting the evolving agglomerate structure during coagulation in the transition regime overpredicts d_m by up to 49%. Thus, interfacing the MPBM with DEM-derived power laws (Equations (1) and (2)) is essential to account for the realistic agglomerate structure and accurately estimate the d_m dynamics so that they are in excellent agreement with data.

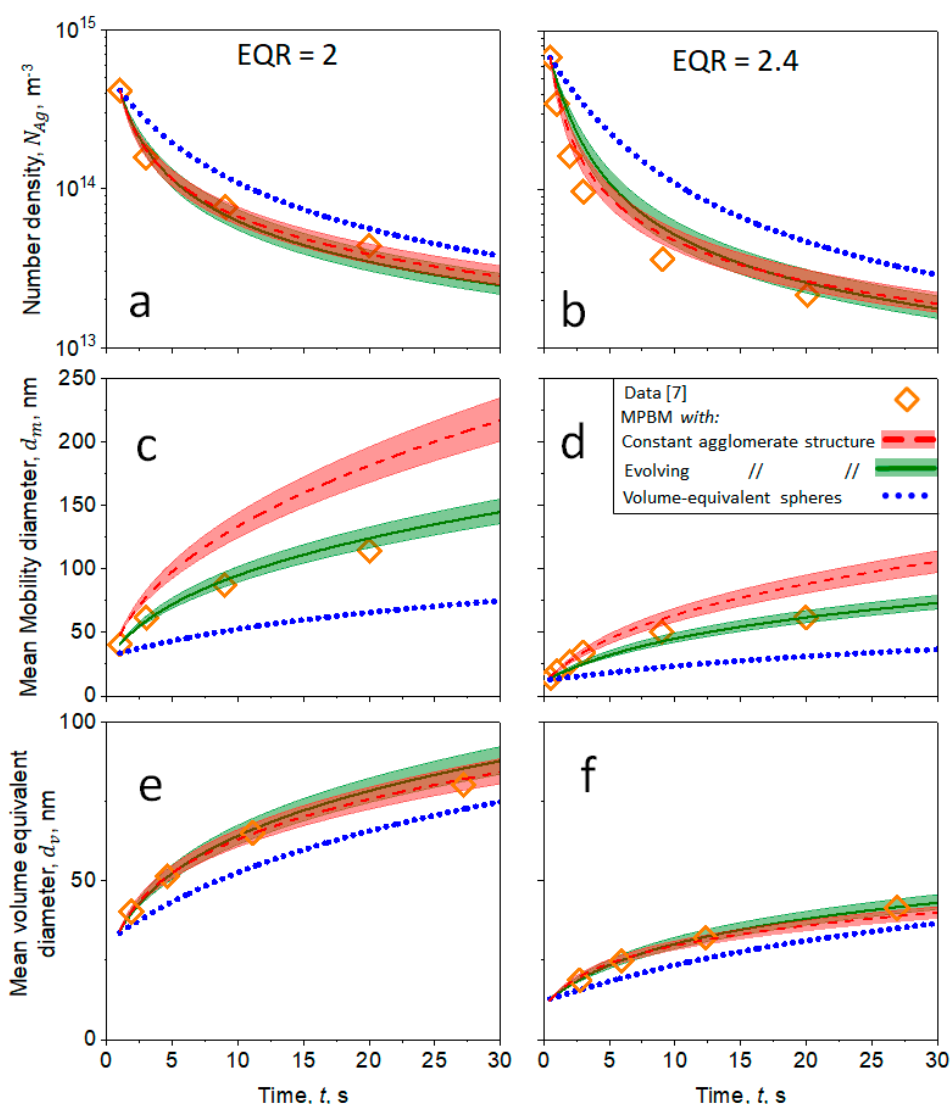


Figure 7. Evolution of agglomerate (a,b) N_{Ag} , (c,d) d_m and (e,f) d_v as a function of t measured (diamonds) for soot sampled from premixed flames with EQR = 2 (a,c,e) and 2.4 (b,d,f) [7] compared to those derived by the MPBM (lines, shades) for volume-equivalent spheres (dotted lines) or agglomerates with constant (broken lines) and evolving morphology (solid line). All sub-figures (a–f) share the same legend.

4. Conclusions

A simple monodisperse population balance model (MPBM) is derived here for the agglomeration of nanoparticles in the transition regime. The MPBM uses relations derived from detailed discrete element modeling (DEM) simulations in order to obtain the evolving structure of agglomerates quantified by their mobility and gyration diameters. As a result, the DEM-derived collision frequency, β , that accounts for the agglomerate size polydispersity is $82 \pm 35\%$ larger than that of monodisperse agglomerates and in excellent agreement with measurements of flame-made TiO₂ nanoparticles. Therefore, the N_{Ag} , d_m and d_v derived by the MPBM, accounting for the evolving fractal-like structure of agglomerates (Equations (1) and (2)) and the impact of their polydispersity on β (Equation (9)), are on par with those obtained by detailed DEM simulations for both monodisperse and polydisperse primary particles coagulating at pressures $P = 1\text{--}5$ bar. Most importantly, the soot agglomerate N_{Ag} , d_m and d_v derived during coagulation at low temperatures are in excellent agreement with data from various premixed flame conditions. In contrast, neglecting the fractal-like morphology of agglomerates or their evolving structure during

coagulation results in an underestimation or overestimation of the mean d_m by up to 93% or 49%, respectively. Thus, the MPBM derived here accounting for the realistic nanoparticle agglomerate structure can be readily interfaced with CFD in order to accurately simulate the agglomeration dynamics of nanoparticles at high pressures or low temperatures that are present in engines or during sampling and atmospheric aging.

Supplementary Materials: The following are available online at <https://www.mdpi.com/article/10.3390/ma14143882/s1>, Figure S1: Evolution of (a) collision frequency, β , (b) number density, N_{Ag} , (c) mean mobility, d_m , and (d) volume-equivalent, d_v , diameters as a function of time, t , for agglomerates consisting of monodisperse primary particles with $d_p = 10$ (solid lines), 20 (broken lines) and 40 nm (dotted lines) derived by DEM (thick lines) and MPBM (thin lines and shaded areas) at $T = 1830$ K and $P = 1$ bar. The MPBM-derived agglomerate dynamics are in excellent agreement with those obtained by DEM for the wide range of d_p studied here. Figure S2: Evolution of (a) β , (b) N_{Ag} , (c) d_m , and (d) d_v as a function of t for monodisperse primary particles with initial $N_{Ag,0} = 2 \cdot 10^{15}$ (solid lines), $2 \cdot 10^{17}$ (broken lines) or $2 \cdot 10^{19} \text{ m}^{-3}$ (dotted lines) and $d_p = 20$ nm derived by DEM (thick lines) and MPBM (thin lines and shaded areas) at $T = 1830$ K and $P = 1$ bar. The MPBM-derived agglomeration dynamics are in excellent agreement with those obtained by DEM for $N_{Ag,0}$ and (incubation) residence times spanning 6 and 8 orders of magnitude, respectively.

Author Contributions: Conceptualization, G.A.K. and M.R.K.; Formal analysis, G.A.K. and M.R.K.; Funding acquisition, M.R.K.; Investigation, G.A.K. and M.R.K.; Methodology, M.R.K.; Software, G.A.K. and M.R.K.; Validation, G.A.K. and M.R.K.; Visualization, G.A.K. and M.R.K.; Writing—original draft, G.A.K. and M.R.K.; Writing—review & editing, G.A.K. and M.R.K. All authors have read and agreed to the published version of the manuscript.

Funding: The research leading to these results has received funding from Canada Research Chairs Program (Grant # CRC-2019-232527), Natural Sciences and Engineering Research Council of Canada (Discovery Grant # RGPIN-2019-06330 and -Early Career Supplemental Award # DGEGR-2019-00220), from the Particle Technology Laboratory, ETH Zurich, Stavros Niarchos Foundations (ETH-08 14-2) and in part by Swiss National Science Foundation (200020_182668, 250320_163243 and 206021_170729).

Institutional Review Board Statement: Not applicable.

Informed Consent Statement: Not applicable.

Data Availability Statement: All the data is available within the manuscript.

Acknowledgments: We gratefully acknowledge insightful comments and suggestions from Sotiris Pratsinis.

Conflicts of Interest: The authors declare that they have no conflict of interest.

Nomenclature

d_c	Collision diameter, m
d_g	Gyration diameter, m
d_m	Mobility diameter, m
d_p	Primary particle diameter, m
D_f	Fractal dimension
D_{fm}	Mass-mobility exponent
k_B	Boltzmann constant, $\text{m}^2\text{kg}/\text{s}^2/\text{K}$
k_n	Fractal prefactor
k_m	Mass-mobility prefactor
Kn	Knudsen number
m_{Ag}	Single agglomerate mass, kg
n_p	Number of primary particles per agglomerate

N_{Ag}	Agglomerate number density, m^{-3}
P	Gas pressure, $kg/s^2/m$
R	Universal gas constant, $m^2kg/s^2/mol/K$
t	Time, s
T	Temperature, K
Greek letters	
β	Collision frequency, m^3/s
ρ	Bulk aerosol density, kg/m^3
ρ_{eff}	Effective aerosol density, kg/m^3
$\sigma_{g,m}$	Geometric standard deviation of d_m distribution
$\sigma_{g,p}$	Geometric standard deviation of d_p distribution

References

- Pratsinis, S.E. Flame aerosol synthesis of ceramic powders. *Prog. Energy Combust. Sci.* **1998**, *24*, 197–219. [[CrossRef](#)]
- Kholghy, M.R.; Kelesidis, G.A.; Pratsinis, S.E. Reactive polycyclic aromatic hydrocarbon dimerization drives soot nucleation. *Phys. Chem. Chem. Phys.* **2018**, *20*, 10926–10938. [[CrossRef](#)] [[PubMed](#)]
- Kelesidis, G.A.; Goudeli, E.; Pratsinis, S.E. Flame synthesis of functional nanostructured materials and devices: Surface growth and aggregation. *Proc. Combust. Inst.* **2017**, *36*, 29–50. [[CrossRef](#)]
- Tsantilis, S.; Pratsinis, S.E. Soft-and hard-agglomerate aerosols made at high temperatures. *Langmuir* **2004**, *20*, 5933–5939. [[CrossRef](#)] [[PubMed](#)]
- Friedlander, S.K. *Smoke, Dust, and Haze*; Oxford University Press: New York, NY, USA, 2000.
- Musculus, M.P.; Miles, P.C.; Pickett, L.M. Conceptual models for partially premixed low-temperature diesel combustion. *Prog. Energy Combust. Sci.* **2013**, *39*, 246–283. [[CrossRef](#)]
- Maricq, M.M. Coagulation dynamics of fractal-like soot aggregates. *J. Aerosol. Sci.* **2007**, *38*, 141–156. [[CrossRef](#)]
- Capes, G.; Johnson, B.; McFiggans, G.; Williams, P.; Haywood, J.; Coe, H. Aging of biomass burning aerosols over West Africa: Aircraft measurements of chemical composition, microphysical properties, and emission ratios. *J. Geophys. Res. Atmos.* **2008**, *113*. [[CrossRef](#)]
- Otto, E.; Stratmann, F.; Fissan, H.; Vemury, S.; Pratsinis, S.E. Quasi-Self-Preserving Log-Normal Size Distributions in the Transition Regime. *Part. Part. Syst. Charact.* **1994**, *11*, 359–366. [[CrossRef](#)]
- Kelesidis, G.A.; Goudeli, E.; Pratsinis, S.E. Morphology and mobility diameter of carbonaceous aerosols during agglomeration and surface growth. *Carbon* **2017**, *121*, 527–535. [[CrossRef](#)]
- Goudeli, E.; Eggersdorfer, M.L.; Pratsinis, S.E. Aggregate characteristics accounting for the evolving fractal-like structure during coagulation and sintering. *J. Aerosol. Sci.* **2015**, *89*, 58–68. [[CrossRef](#)]
- Goudeli, E.; Eggersdorfer, M.L.; Pratsinis, S.E. Coagulation of agglomerates consisting of polydisperse primary particles. *Langmuir* **2016**, *32*, 9276–9285. [[CrossRef](#)] [[PubMed](#)]
- Sun, B.; Rigopoulos, S.; Liu, A. Modelling of soot coalescence and aggregation with a two-population balance equation model and a conservative finite volume method. *Combust. Flame* **2021**, *229*, 111382. [[CrossRef](#)]
- Kholghy, M.R.; Veshkini, A.; Thomson, M.J. The core-shell internal nanostructure of soot—A criterion to model soot maturity. *Carbon* **2016**, *100*, 508–536. [[CrossRef](#)]
- Mueller, M.E.; Blanquart, G.; Pitsch, H. Hybrid method of moments for modeling soot formation and growth. *Combust. Flame* **2009**, *156*, 1143–1155. [[CrossRef](#)]
- Kruis, F.E.; Kusters, K.A.; Pratsinis, S.E.; Scarlett, B. A simple model for the evolution of the characteristics of aggregate particles undergoing coagulation and sintering. *Aerosol Sci. Technol.* **1993**, *19*, 514–526. [[CrossRef](#)]
- Liu, A.; Rigopoulos, S. A conservative method for numerical solution of the population balance equation, and application to soot formation. *Combust. Flame* **2019**, *205*, 506–521. [[CrossRef](#)]
- Saggese, C.; Ferrario, S.; Camacho, J.; Cuoci, A.; Frassoldati, A.; Ranzi, E.; Wang, H.; Faravelli, T. Kinetic modeling of particle size distribution of soot in a premixed burner-stabilized stagnation ethylene flame. *Combust. Flame* **2015**, *162*, 3356–3369. [[CrossRef](#)]
- Mann, G.; Carlaw, K.; Spracklen, D.; Ridley, D.; Manktelow, P.; Chipperfield, M.; Pickering, S.; Johnson, C. Description and evaluation of GLOMAP-mode: A modal global aerosol microphysics model for the UKCA composition-climate model. *Geosci. Model Dev.* **2010**, *3*, 519–551. [[CrossRef](#)]
- Goudeli, E.; Eggersdorfer, M.L.; Pratsinis, S.E. Coagulation–Agglomeration of fractal-like particles: Structure and self-preserving size distribution. *Langmuir* **2015**, *31*, 1320–1327. [[CrossRef](#)]
- Kelesidis, G.A.; Goudeli, E. Self-preserving size distribution and collision frequency of flame-made nanoparticles in the transition regime. *Proc. Combust. Inst.* **2021**, *38*, 1233–1240. [[CrossRef](#)]
- Kelesidis, G.A.; Furrer, F.M.; Wegner, K.; Pratsinis, S.E. Impact of humidity on silica nanoparticle agglomerate morphology and size distribution. *Langmuir* **2018**, *34*, 8532–8541. [[CrossRef](#)] [[PubMed](#)]
- Rissler, J.; Messing, M.E.; Malik, A.I.; Nilsson, P.T.; Nordin, E.Z.; Bohgard, M.; Sanati, M.; Pagels, J.H. Effective density characterization of soot agglomerates from various sources and comparison to aggregation theory. *Aerosol Sci. Technol.* **2013**, *47*, 792–805. [[CrossRef](#)]

24. Maricq, M.M. Examining the relationship between black carbon and soot in flames and engine exhaust. *Aerosol Sci. Technol.* **2014**, *48*, 620–629. [[CrossRef](#)]
25. Isella, L.; Giechaskiel, B.; Drossinos, Y. Diesel-exhaust aerosol dynamics from the tailpipe to the dilution tunnel. *J. Aerosol Sci.* **2008**, *39*, 737–758. [[CrossRef](#)]
26. Rigopoulos, S.; Jones, A.G. Finite-element scheme for solution of the dynamic population balance equation. *AIChE J.* **2003**, *49*, 1127–1139. [[CrossRef](#)]
27. Wan, Z.; You, Z.; Sun, Z.; Yin, W. Method of Taylor expansion moment incorporating fractal theories for Brownian coagulation of fine particles. *Int. J. Nonlinear Sci. Numer. Simul.* **2012**, *13*, 459–467. [[CrossRef](#)]
28. Dimakopoulos, Y.; Kelesidis, G.; Tsouka, S.; Georgiou, G.C.; Tsamopoulos, J. Hemodynamics in stenotic vessels of small diameter under steady state conditions: Effect of viscoelasticity and migration of red blood cells. *Biorheology* **2015**, *52*, 183–210. [[CrossRef](#)] [[PubMed](#)]
29. Kholghy, M.R.; Schumann, A. A Simple Model for Gas-Phase Synthesis of Nickel Nanoparticles. *Energy Fuels* **2021**, *35*, 5383–5391. [[CrossRef](#)]
30. Tsantilis, S.; Kammler, H.K.; Pratsinis, S.E. Population balance modeling of flame synthesis of titania nanoparticles. *Chem. Eng. Sci.* **2002**, *57*, 2139–2156. [[CrossRef](#)]
31. Xiong, Y.; Akhtar, M.K.; Pratsinis, S.E. Formation of agglomerate particles by coagulation and sintering—Part II. The evolution of the morphology of aerosol-made titania, silica and silica-doped titania powders. *J. Aerosol Sci.* **1993**, *24*, 301–313. [[CrossRef](#)]
32. Kholghy, M.R.; Kelesidis, G.A. Surface growth, coagulation and oxidation of soot by a monodisperse population balance model. *Combust. Flame* **2021**, *227*, 456–463. [[CrossRef](#)]
33. Heine, M.; Pratsinis, S.E. Brownian coagulation at high concentration. *Langmuir* **2007**, *23*, 9882–9890. [[CrossRef](#)] [[PubMed](#)]
34. Allen, M.P.; Tildesley, D.J. *Computer Simulation of Liquids*; Oxford University Press: New York, NY, USA, 2017.
35. Kelesidis, G.A.; Kholghy, M.R.; Zuercher, J.; Robertz, J.; Allemann, M.; Duric, A.; Pratsinis, S.E. Light scattering from nanoparticle agglomerates. *Powder Technol.* **2020**, *365*, 52–59. [[CrossRef](#)]
36. Kelesidis, G.A.; Pratsinis, S.E. A perspective on gas-phase synthesis of nanomaterials: Process design, impact and outlook. *Chem. Eng. Sci.* **2021**, *421*, 129884. [[CrossRef](#)]
37. Eggersdorfer, M.L.; Gröhn, A.J.; Sorensen, C.; McMurry, P.H.; Pratsinis, S.E. Mass-mobility characterization of flame-made ZrO₂ aerosols: Primary particle diameter and extent of aggregation. *J. Colloid Interface Sci.* **2012**, *387*, 12–23. [[CrossRef](#)] [[PubMed](#)]
38. Meakin, P. Fractal aggregates. *Adv. Colloid Interface Sci.* **1987**, *28*, 249–331. [[CrossRef](#)]
39. Katzer, M.; Weber, A.P.; Kasper, G. Collision kinetics and electrostatic dispersion of airborne submicrometer fractal agglomerates. *J. Colloid Interface Sci.* **2001**, *240*, 67–77. [[CrossRef](#)] [[PubMed](#)]
40. Medalia, A.I. Dynamic shape factors of particles. *Powder Technol.* **1971**, *4*, 117–138. [[CrossRef](#)]
41. Wang, G.; Sorensen, C. Diffusive mobility of fractal aggregates over the entire Knudsen number range. *Phys. Rev. E* **1999**, *60*, 3036. [[CrossRef](#)]
42. Eggersdorfer, M.L.; Pratsinis, S.E. Agglomerates and aggregates of nanoparticles made in the gas phase. *Adv. Powder Technol.* **2014**, *25*, 71–90. [[CrossRef](#)]
43. Gwaze, P.; Schmid, O.; Annegarn, H.J.; Andreae, M.O.; Huth, J.; Helas, G. Comparison of three methods of fractal analysis applied to soot aggregates from wood combustion. *J. Aerosol Sci.* **2006**, *37*, 820–838. [[CrossRef](#)]
44. Sotiriou, G.A.; Etterlin, G.D.; Spyrogianni, A.; Krumeich, F.; Leroux, J.-C.; Pratsinis, S.E. Plasmonic biocompatible silver–gold alloyed nanoparticles. *Chem. Comm.* **2014**, *50*, 13559–13562. [[CrossRef](#)] [[PubMed](#)]
45. Fuchs, N.A.; Daisley, R.; Fuchs, M.; Davies, C.; Straumanis, M. The mechanics of aerosols. *Phys. Today* **1965**, *18*, 73. [[CrossRef](#)]
46. Cussler, E.L. *Diffusion: Mass Transfer in Fluid Systems*; Cambridge University Press: Cambridge, UK, 2009.
47. Xu, F.; Sunderland, P.; Faeth, G. Soot formation in laminar premixed ethylene/air flames at atmospheric pressure. *Combust. Flame* **1997**, *108*, 471–493. [[CrossRef](#)]